The Micro-optical Disc Electrode Part 2: Theory for the Transport Limited, Steady State Photocurrent[§]

Fabrice P.L.Andrieux [a], Colin Boxall [b], Danny O'Hare [c]

[a] Centre for Materials Science, University of Central Lancashire, Preston PR1 2HE, UK; email: fandrieux@uclan.ac.uk

[b] Centre for Materials Science, University of Central Lancashire, Preston PR1 2HE, UK; email: cboxall@uclan.ac.uk

[c] Department of Bioengineering, Imperial College, London SW7 2BP, UK; email: d.ohare@imperial.ac.uk

Corresponding Author:

Dr Colin Boxall

Centre for Materials Science, University of Central Lancashire, Preston PR1 2HE, UK

tel.: +44 1772 893530;

fax: +44 01772 892996

email: cboxall@uclan.ac.uk

[§]Part 1 presented in ref 1

Abstract

The Micro-Optical Ring Electrode (MORE) is a photoelectrochemical device based on a ring microelectrode that uses the insulating material interior to the ring electrode as a light guide. In this paper, we derive asymptotic analytical expressions for the steady state, transport limited photocurrent generated at MOREs with thin microrings ((ring inner radius)/(ring outer radius) values > 0.99) for two general types of photoelectrochemical system (a) the PE (Photophysical-Electrochemical) system, wherein the photoexcited species itself is directly detected on the ring; and (b) the PCE (Photophysical-Chemical-Electrochemical) system, wherein the photoexcited species undergoes a homogeneous electron transfer reaction prior to electrochemical detection. The expressions are generated by exploiting the properties of discontinuous integrals of Bessel Functions to solve the diffusion equation for the photogenerated electroactive species both inside and outside the beam. The resultant solutions are then matched at the beam surface. The expressions themselves are used to design experimental protocols that allow for the complete characterization of the photoelectrochemical kinetics of a system and are tested by using them to interpret the results of a MORE study of the photoelectrochemical behaviour of the $Ru(bipy)_3^{2+}/Fe^{3+}$ photosensitiser / quenching agent system. The value of the Stern-Volmer constant for the quenching of photoexcited $Ru(bipy)_3^{2+}$ by Fe^{3+} so obtained (0.36 m^3 mol^{-1}) compares favourably with the value obtained from fluorescence measurements (0.9 m^3 mol^{-1}).

Keywords

Photoelectrochemistry; Electroanalysis; Ring microelectrode; Microring; Optical electrode; Photoelectrode.

1. Introduction

Microring electrodes find use in a wide range of electrochemical applications [1-19]. This is primarily because their large perimeter-to-area ratio results in an enhanced material flux to the electrode surface, leading to higher current densities and improved temporal resolution in the study of reactions with fast chemical and electrochemical kinetics. Based on a ring microelectrode and using the insulator interior to the ring as a light guide, the MORE (Fig. 1) is a photoelectrochemical device capable of delivering light *via* a fiber optic directly to the region of electrochemical measurement, so allowing microelectrochemical study of systems with complex photochemistries. As such, it exploits the enhanced temporal resolution of microrings in that many photogenerated species are comparatively short-lived.

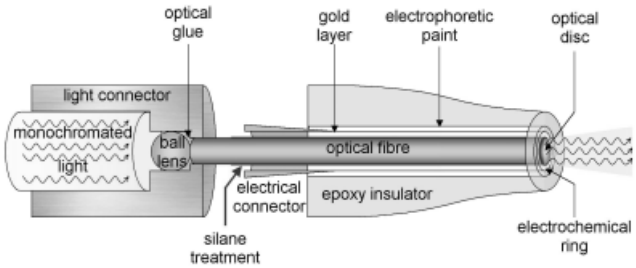

Fig. 1. Schematic cross section of tip of MORE and home-made light coupling unit.

Derivation of analytical expressions for the steady state, transport limited current to microrings in the dark is a challenging problem because the diffusion equation must be solved subject to mixed boundary conditions (i.e. the flux is specified at one part of a surface and the concentration on another) [20]. The majority of (semi-) analytical approaches to solving the dark problem do so for so called “thin rings” ((ring inner radius, a)/(outer radius, b) values > 0.91 [20-23]), assuming a constant flux over the electrode surface. Notable exceptions to this are the work of Philips *et al.* [24], Tallman *et al.* [25-28] and Wu *et al.* [29-30]. More recently, Compton *et al.* [13] have used a finite difference numerical method to produce current results for both

chronoamperometry and linear sweep voltammetry at microrings of intermediate thickness.

Numerical simulations of the dark behaviour of microrings notwithstanding, in modelling the photocurrent behaviour of the MORE, we have opted for an analytical approach as the availability of simple analytical solutions greatly facilitates the analysis of experimental data. Following our earlier approach in modelling the photocurrent behavior of semi-transparent optical disc electrodes (ODEs) [31,32], we chose to model the photoelectrochemical response at the MORE of two types of photosystems: (i) a sensitiser, S, is photoexcited to form S* (Eq. (1a)) with quantum efficiency ϕ. This may then either relax back to form S (Eq. (1a)) or be detected at the electrode which, for the purposes of this communication, we have shown as an oxidation (a PE process – **P**hotophysical-**E**lectrochemical):

solution: $$S \xrightarrow{h\nu} S^* \xrightarrow{k_0} S \qquad (1a)$$

electrode: $$S^* \longrightarrow S^+ + e^- \; ; \; E^0_{S^*/S^+} \qquad (1b)$$

(ii) photoexcitation of S (Eq. (1a)), which may then either relax back or undergo an electron transfer process with a charge scavenger, A, to form S^+ and A^- (Eq. (1c)). Either S^+ or A^- may then be detected at the electrode surface; for the purposes of this communication, we assume the photocurrent is due to reduction of S^+, which may itself undergo some loss reaction (Eq. (1d)), possibly with A^-, to regenerate S (a PCE process - **P**hotophysical **C**hemical **E**lectrochemical):

solution: $$S^* + A \xrightarrow{k_1} S^+ + A^- \qquad (1c)$$

solution: $$S^+ \xrightarrow{k_2} S \qquad (1d)$$

electrode: $$S^+ + e^- \longrightarrow S \; ; \; E^0_{S/S^+} \qquad (1e)$$

where S* is the photoexcited sensitiser, k_0 is a pseudo-first order rate constant (s^{-1}) and k_1 and k_2 are second order rate constants (m^3 mol^{-1} s^{-1}). The models developed will be applicable to the study of homogeneous and microheterogeneous photosystems (such as colloidal semiconductors) that (i) exhibit electrochemical activity and (ii) are not subject to quenching reactions at metal electrode surfaces through double electron transfer mechanisms. As such, these models will find use in the areas of e.g. solar energy conversion [33-36], pollution abatement [37], non-linear optics [38], photo electroanalysis [39], and the study of photoactive drugs for the treatment of cancer [40].

Thus, in this paper, we describe a theoretical treatment for the study of PE and PCE systems using the MORE. For both systems, we generate approximate expressions for the steady state, diffusion limited photocurrent at the MORE and test those expressions using data from the $Ru(bipy)_3^{2+}/Fe^{3+}$ PCE system.

2. Experimental

2.1 Reagents

All chemicals were of analytical grade or better and used as received. Distilled water, produced by a home-made still, was further purified by a deionisation system (E pure model 04642, Barnstead/Thermodyne, Dubuque, Iowa, USA) to a resistivity of 1.8 x 10^5 Ωm. Prior to electrochemical analysis, all reagent solutions were purged for 15 minutes with nitrogen (white spot grade, BOC Ltd., Guildford, Surrey, UK).

2.2 Electrodes, Equipment and Optical Arrangement

MORE fabrication and characterisation have been described elsewhere [1,18,19]. All MOREs had gold rings with an internal ring diameter of 250 μm and a thickness of 5 nm. Illumination was provided by a 900 Watt Xe Arc Lamp (Applied Photophysics, UK) in conjunction with an f/3.4 grating monochromator (Applied Photophysics). The output

of the monochromator was focussed onto one end of a light guide cable (Applied Photophysics), the other end of which was interfaced with the MORE through a home-made light coupling unit (Fig. 1).

All voltammetric measurements were made in a three-electrode arrangement with a saturated calomel electrode (SCE) (EIL, Chertsy, Surrey, UK) as reference and a Pt wire as the counter electrode. The potentiostat used was an Autolab PGSTAT10 computer controlled workstation (Windsor Scientific Ltd., Slough, UK) incorporating a preamplifier (model ECD) for low current measurements. In order to minimise electrical noise, the workstation was powered through a mains filter (Bowthorpe PP3, Maplins, Rayleigh, UK) and all (photo-)electrochemical experiments were conducted with the electrochemical cell placed within a home-made Faraday cage, which also served to exclude ambient light during experiments in the dark. All photocurrent signals with a signal-to noise ratio (S/N) of less than 2 were discarded. All experiments were conducted at room temperature (291 ± 2 K).

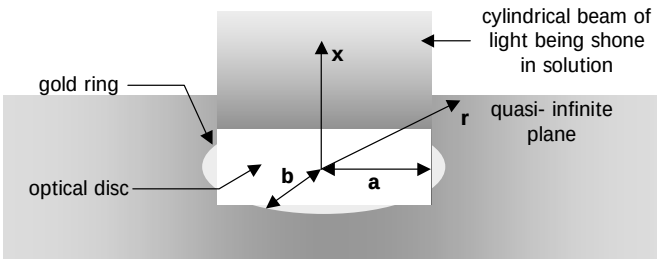

Fig. 2. The cylindrical polar geometry of the MORE problem

3. Results and Discussion

3.1 Theory for the Transport-Limited, Steady State Photocurrent from a PE System

The system to be modelled is shown in Eq. (1a) and (1b). Fig. 2 illustrates the geometry of the problem wherein x is the perpendicular distance from the plane of the electrode surface and r the radial distance from the centre of the optical disc. The optical

disc is assumed to be uniformly illuminated by parallel light passing from the disc into solution (see Appendix for the limitations of this assumption). The steady state diffusion equation for S* is set up using the following assumptions [31, 32]:

1.1. The light makes only a small perturbation to [S] (mol m^{-3}), thus not altering the dark current value significantly. This means that the solution does not bleach and I, the flux of light at distance x normal to the electrode surface, is given by $I = I_{ph}\ e^{-\varepsilon_\lambda [S]x}$, where I_{ph} is the flux of light at the electrode surface ((mol photons) m^{-2} s^{-1}) and ε_λ is the absorption coefficient (m^2 mol^{-1}) at wavelength λ.

1.2. The homogeneous loss reaction is pseudo- 1st-order with respect to [S*] with rate coefficient k_0.

1.3 The electron transfer kinetics of S* at the electrode are extremely rapid, the photocurrent being under either mass transport or photochemical kinetic control.

The diffusion equation for S* in cylindrical polar coordinates is then given by

$$D_s \frac{\partial^2 [S^*]}{\partial r^2} + \frac{D_s}{r}\frac{\partial [S^*]}{\partial r} + D_s \frac{\partial^2 [S^*]}{\partial x^2} - k_0 [S^*] + \phi I_{ph} \varepsilon_\lambda [S] e^{-\varepsilon_\lambda [S]x} = 0 \qquad (2a)$$

at r < a, inside the beam and

$$D_s \frac{\partial^2 [S^*]}{\partial r^2} + \frac{D_s}{r}\frac{\partial [S^*]}{\partial r} + D_s \frac{\partial^2 [S^*]}{\partial x^2} - k_0 [S^*] = 0 \qquad (2b)$$

at r > a, outside the beam. As well as a and b, the system has two characteristic lengths:

the thickness of the reaction layer: $X_{k,0} = (D_S / k_0)^{1/2}$ (3a)

the thickness of the absorbance layer: $X_\varepsilon = (\varepsilon_\lambda [S])^{-1}$ (3b)

Solution of Eqs. (2) may be simplified by use of the following dimensionless variables:

$$\chi = \frac{x}{X_{k,0}} \qquad \rho = \frac{r}{X_{k,0}} \qquad U = \frac{D_S [S^*]}{\phi' I_{ph} X_\varepsilon} \qquad \gamma = \frac{X_{k,0}}{X_\varepsilon} \qquad (4a,b,c,d)$$

giving, at $\rho < \rho_0$ inside, and $\rho > \rho_0$ outside the beam respectively:

$$\frac{\partial^2 U}{\partial \rho^2} + \frac{1}{\rho}\frac{\partial U}{\partial \rho} + \frac{\partial^2 U}{\partial \chi^2} - U + \gamma^2 e^{-\gamma\chi} = 0 \qquad (5a)$$

$$\frac{\partial^2 U}{\partial \rho^2} + \frac{1}{\rho}\frac{\partial U}{\partial \rho} + \frac{\partial^2 U}{\partial \chi^2} - U = 0 \qquad (5b)$$

where the normalized inner and outer radii of the ring are given by

$$\rho_o = a / X_{k,0} \text{ and } \rho_1 = b / X_{k,0} \qquad (6a,b)$$

We are investigating a diffusion transport-limited oxidative process given by Eq. (1b). Thus, the normalized boundary conditions for the solution of Eqs. (5) are given in Table 1. However, in solving Eqs. (5), it is instructive to first consider the concentration field generated at the MORE when the microring is switched off i.e. no electrochemistry is occurring at the electrode surface. If it is further assumed that I is invariant with x as a result of low [S] and / or low ε_λ, then Eqs (5) can be rewritten for inside ($\rho < \rho_0$) and outside the beam ($\rho > \rho_0$) as follows

$$\frac{\partial^2 U}{\partial \rho^2} + \frac{1}{\rho}\frac{\partial U}{\partial \rho} - U + \gamma^2 = 0 \qquad (7a)$$

$$\frac{\partial^2 U}{\partial \rho^2} + \frac{1}{\rho}\frac{\partial U}{\partial \rho} - U = 0 \qquad (7b)$$

Eqs. (7) have the form of Bessel's modified equation [41,42], general solutions being:

$$\text{at } \rho<\rho o: \quad U = \gamma^2 + D_1 I_0(\rho) + E_1 K_0(\rho) \qquad (8a)$$

$$\text{at } \rho>\rho o: \quad U = D_2 I_0(\rho) + E_2 K_0(\rho) \qquad (8b)$$

where $I_m(z)$ is a modified Bessel function of the 1st kind, order m and $K_m(z)$ is a modified Bessel function of the 2nd kind, order m. D_1, E_1, D_2 and E_2 are arbitrary constants of integration. Application of boundary condition B1 indicates $E_1 = D_2 = 0$. Noting that the Wronskian of $I_0(\rho_0)$ and $K_0(\rho_0)$ can be written as [43]:

U is finite over all space		(B1)
At $\rho = 0$ and $0 < \chi < \infty$	$\left(\frac{\partial U}{\partial \rho}\right)_{\rho=0} = 0$	(B2)
When $\rho \to \infty$ and $0 < \chi < \infty$	$\left(\frac{\partial U}{\partial \rho}\right)_{\rho\to\infty} \to 0\,;\ U \to 0$	(B3)
At $\chi \to \infty$ and $0 < \rho < \infty$	$\left(\frac{\partial U}{\partial \chi}\right)_{\chi\to\infty} = 0$	(B4)
At $\rho = \rho_0$ $U_{\text{inside beam}} = U_{\text{outside beam}}$ &	$\left(\frac{\partial U}{\partial \rho}\right)_{\text{inside beam}} = \left(\frac{\partial U}{\partial \rho}\right)_{\text{outside beam}}$	(B5)
When ring is switched off i.e. no electrochemistry at electrode surface		
At $\chi = 0$ and for $0 < \rho < \infty$	$\left(\frac{\partial U}{\partial \chi}\right)_{\chi=0} = 0$	(B6)
When ring is switched on:		
At χ=0 and $\rho_0<\rho<\rho_1$:	$\left(\frac{\partial U}{\partial \chi}\right)_{\chi=0} \neq 0$; and U = 0	(B7a)
At χ=0 and $0<\rho<\rho_0$ & $\rho_1<\rho<\infty$	$\left(\frac{\partial U}{\partial \chi}\right)_{\chi=0} = 0$	(B7b)

Table 1. Normalised boundary conditions for the solution of Eqs. (5).

$$W\{I_0(\rho_0),\ K_0(\rho_0)\} = I_1(\rho_0)K_0(\rho_0) + I_0(\rho_0)K_1(\rho_0) = \frac{1}{\rho_0} \qquad (9)$$

then application of boundary condition B5 to Eqs. (8) gives:

at $\rho<\rho_0$, ring off: $$U_{\text{inside}} = \gamma^2[1 - \rho_0 K_1(\rho_0) I_0(\rho)] \qquad (10a)$$

at $\rho>\rho_0$, ring off: $$U_{\text{outside}} = \gamma^2 \rho_0 I_1(\rho_0) K_0(\rho) \qquad (10b)$$

Fig. 3 shows the χ-independent concentration profile of the photogenerated species as a function of the normalised radial distance from the centre of the disc when $\gamma<1$, $\rho_0 = 2.5$.

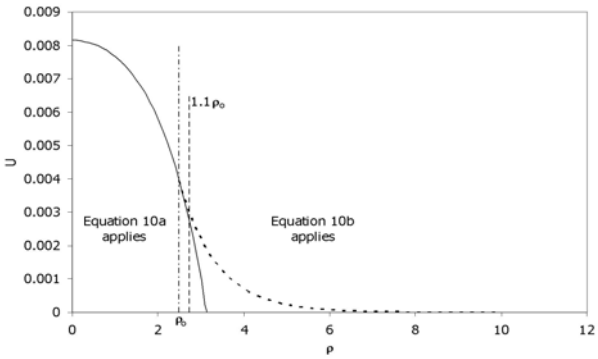

Fig. 3. Concentration profile of photogenerated species (as U/γ^2) at MORE surface inside and outside the beam, calculated using Eqs. (10) when $\gamma<1$ and the ring is off. Calculated for $\rho_0=2.5$ and $\gamma=0.1$. Solid line represents U/γ^2 as given by Eq. (10a), broken line as given by Eq. (10b).

We now move on to discuss the solution of Eqs. (5) when the ring electrode is switched on i.e. S* is consumed at the electrode surface under diffusion control. We again assume that I is invariant with χ i.e. $\gamma < 1$. Inside the beam, Eq. (5a) then becomes:

$$\frac{\partial^2 U}{\partial \rho^2} + \frac{1}{\rho}\frac{\partial U}{\partial \rho} + \frac{\partial^2 U}{\partial \chi^2} - U + \gamma^2 = 0 \qquad (11)$$

Outside the beam, Eq. (5b) is unchanged. Semi analytical solutions to Eqs. (11) and (5b) may be achieved by following an analogous approach to that adopted when the ring is off. However, Eq. (5b) must be solved using the discontinuous boundary conditions B7, the resultant solution matching at $\rho = \rho_0$ producing a set of dual integral equations that appear analytically intractable. This difficulty may be circumvented by assuming that Eq. (11) applies in the range $0 < \rho < \rho_1$ rather than $0 < \rho < \rho_0$ i.e. that it applies over the ring, despite the fact that no photogeneration occurs in that space.

This assumption can be defended as follows. Returning to Eqs. (10) and Fig. 3, we can calculate the error produced in the calculated values of the concentration field when

Eq. (10a) rather than Eq. (10b) is applied to the space defined by $\rho_0 < \rho < \rho_1$. At a median value of ρ_0 such as $\rho_0 = 2.5$ and $\rho_1 = 1.1\rho_0$ (i.e. the thickest ring that still conforms with the definition of a thin ring [21]), use of Eq. (10a) at $\rho_0 < \rho < \rho_1$ gives rise to >10% error in the calculated concentration of the photoexcited species in that space. However, our MOREs have ρ_0/ρ_1 values > 0.99 i.e. $\rho_1 < 1.01\rho_0$. When dealing with such very thin rings, the error in the value of [S*] in the space above the ring when calculated using Eq. (10a) instead of (10b) is less than 1.2% if $\rho_0 < 10$ and 5.1% if $\rho_0 < 20$. Fig. 4 shows the percentage error as a function of ρ_0 for a ring where $\rho_1 = 1.01\rho_0$ (i.e. the thickest ring that still conforms with our definition of a very thin ring). Thus, if $\rho_0/\rho_1 > 0.99$ and $\rho_0 < 20$, then the concentration field over the ring can be considered as being determined by Eq. (7a) (electrochemistry off) and Eq. (11) (electrochemistry on). We shall now solve Eq. (11) for $0 < \rho < \rho_1$ with these restrictions in mind.

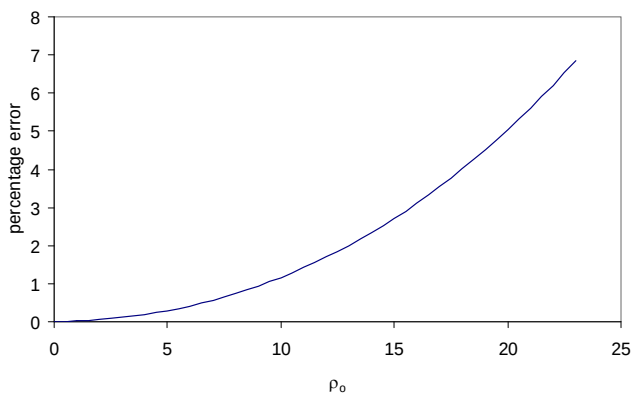

Fig. 4. Percentage error associated with using Eq. (10a) rather than Eq. (10b) to calculate concentration of photogenerated species (as U) in the space defined by $\rho_0 < \rho < 1.01\rho_0$ over an illuminated MORE with the electrochemical ring switched off.

For any λ, $J_0(\lambda\rho)e^{-\left(1+\lambda^2\right)^{1/2}\chi}$ is a solution of the homogeneous part of Eq. (11), where λ is an arbitrary real non-zero constant and $J_m(z)$ is a Bessel function of the 1st

kind, order m. By application of boundary condition B7b at $\rho < \rho_0$, it can be shown that the general solution is of the form

$$U = \gamma^2 + C\,I_0(\rho) + C'\int_0^\infty f(\lambda)J_0(\lambda\rho)e^{-\left(1+\lambda^2\right)^{1/2}\chi}\,d\lambda - \qquad (12)$$

C and C' are arbitrary constants of integration and f(λ) must satisfy boundary conditions B7. The integral Eq. 12 must be discontinuous at $\rho = \rho_0$ as B7 requires that

$$\left(\frac{\partial U}{\partial \chi}\right)_{\chi=0} = \int_0^\infty f(\lambda)J_0(\lambda\rho)\left(1+\lambda^2\right)^{1/2}\,d\lambda - \;=\; 0 \text{ for } 0 < \rho < \rho_0$$

while for $\rho > \rho_0$ the gradient is arbitrary except that it cannot be zero. The discontinuous integrals [44]

$$\int_0^\infty J_0(\lambda\rho)\cos(\lambda\rho_0)\,d\lambda - = 0 \text{ for } 0 < \rho < \rho_o \text{ (inside the beam)} \qquad (13a)$$

$$\int_0^\infty J_0(\lambda\rho)\cos(\lambda\rho_0)\,d\lambda - \neq 0 \text{ for } \rho > \rho_o \text{ (outside the beam)} \qquad (13b)$$

satisfy condition B7 provided $f(\lambda)\left(1+\lambda^2\right)^{1/2} = \cos(\lambda\rho_o)$ i.e. we obtain the solution:

$$U = \gamma^2 + C\,I_0(\rho) + C'\int_0^\infty \frac{\cos(\lambda\rho_0)}{\left(1+\lambda^2\right)^{1/2}} J_0(\lambda\rho)e^{-\left(1+\lambda^2\right)^{1/2}\chi}\,d\lambda \qquad (14)$$

Application of boundary condition B7a at $\chi=0$, $\rho=\rho_0$ gives

$$U = \gamma^2 + C\,I_0(\rho) - \left(\gamma^2 + CI_0(\rho_0)\right)\frac{\displaystyle\int_0^\infty \frac{\cos(\rho_0\lambda)}{\left(1+\lambda^2\right)^{1/2}} J_0(\lambda\rho)e^{-\left(1+\lambda^2\right)^{1/2}\chi}\,d\lambda}{\displaystyle\int_0^\infty \frac{\cos(\lambda\rho_0)J_0(\lambda\rho_0)}{\left(1+\lambda^2\right)^{1/2}}\,d\lambda} \qquad (15)$$

Now as $\chi\to\infty$, $e^{-\left(1+\lambda^2\right)^{1/2}\chi} \to 0$ and U is finite. Therefore at ρ_0, $\chi\to\infty$ we can write

$$U = \gamma^2 + C\,I_0(\rho_0) \qquad (16)$$

At $\chi \to \infty$, perturbations in the concentration field due to depletion of S* at the electrode will be minimal and Eq. (8b) will apply outside the beam. In fact, Eq. (16) is analogous to Eq. (8a). Concentration and concentration gradient matching for Eqs. (16) & (8b) at the beam surface then gives $C = -\gamma^2 \rho_0 K_1(\rho_0)$ and

$$U = \gamma^2 \left\{ 1 - \rho_0 K_1(\rho_0) I_0(\rho) - \left(1 - \rho_0 K_1(\rho_0) I_0(\rho_0)\right) \frac{\int_0^\infty \frac{\cos(\rho_0 \lambda)}{\left(1+\lambda^2\right)^{1/2}} J_0(\lambda\rho) e^{-\left(1+\lambda^2\right)^{1/2}\chi} \, d\lambda}{\int_0^\infty \frac{\cos(\lambda\rho_0) J_0(\lambda\rho_0)}{\left(1+\lambda^2\right)^{1/2}} \, d\lambda} \right\} \quad (17)$$

Substitution of Eq. (17) into Eq. (11) confirms that it is a solution of that equation. Fig. 5 shows a plot of [S*] (as U/γ^2) as a function of ρ and χ when the ring is on, ρ_0=2.5, γ=0.5.

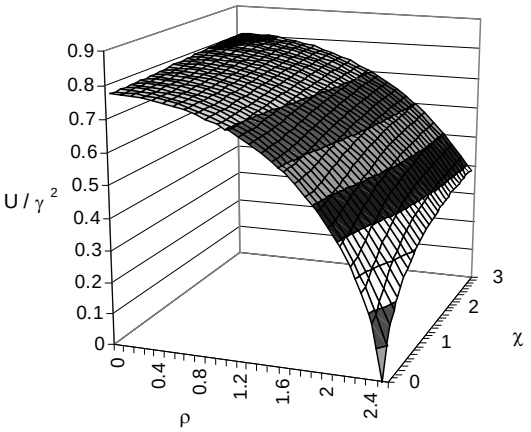

Fig. 5. Concentration profile of photogenerated species (as U / γ^2) at the MORE surface, as a function of ρ and χ, calculated using Eq. (17) when ρ_0=2.5 and γ=0.5 and the electrochemical ring is switched on.

From Fick's first law, the photocurrent is determined by integrating $\left(\frac{\partial U}{\partial \chi}\right)_{\chi=0}$ over the range $\rho_0 < \rho < \rho_1$. The form of Eq. (17) makes the resultant expression cumbersome to use. However, inspection of the form of $\int_0^\infty \frac{\cos(\lambda\rho_0) J_0(\lambda\rho_0)}{\left(1+\lambda^2\right)^{1/2}} \, d\lambda$ shows that

$$\int_0^\infty \frac{\cos(\lambda\rho_0)J_0(\lambda\rho_0)}{\left(1+\lambda^2\right)^{1/2}}\,d\lambda \quad \approx \quad \frac{1.03}{(\rho_0)^{1/2}} \tag{18}$$

with error < 4% for ρ_0 >1 and < 2.6% for ρ_0>2. Noting that

$$\int_0^\infty \cos(\lambda\rho_0)\,J_0(\lambda\rho)\,d\lambda - \;=\frac{1}{\left(\rho^2-\rho_0{}^2\right)^{1/2}} \text{ when } \rho > \rho_0 \text{ [44]}$$

substitution of Eq. (18) into Eq. (17), differentiation and substitution of the result in terms of the original variables into

$$\frac{i}{nFD_S} = 2\pi\int_a^b\left(\frac{\partial[S^*]}{\partial x}\right)_{x=0} r\cdot dr$$

leads, upon integration, to an expression for the photocurrent when 20 > ρ_0 > 1 & γ < 1:

$$i = \frac{2nFD_S\pi\phi I_{ph}\varepsilon_\lambda[S]}{1.03k_0}\left(\frac{a}{X_{k,0}}\right)^{1/2}\left\{1 - \frac{a}{X_{k,0}}K_1\left(\frac{a}{X_{k,0}}\right)I_0\left(\frac{a}{X_{k,0}}\right)\right\}\left(b^2-a^2\right)^{1/2} \tag{19}$$

Further simplification can be achieved by noting that, when ρ_0 > 1 [45]:

$$K_1(\rho_0) \approx \left(\frac{\pi}{2\rho_0}\right)^{1/2} e^{-\rho_0}\left(1+\frac{3}{8\rho_0}\right) \text{ and } I_0(\rho_0) \approx \left(\frac{1}{2\rho_0\pi}\right)^{1/2} e^{+\rho_0}\left(1+\frac{1}{8\rho_0}\right)$$

with error < 4% in each case. Under these conditions, Eq. (19) can be written as:

$$i \;=\; \frac{nFD_S^{3/4}\pi a^{1/2}I_{ph}\varepsilon_\lambda[S]\left(b^2-a^2\right)^{1/2}}{1.03}\;\left\{\frac{\phi}{k_0^{3/4}}\right\}\;\left\{1-\frac{1}{2a}\left(\frac{D_S}{k_0}\right)^{1/2}\right\} \tag{20}$$

with an overall error < 5%. Inspection of Eqs. (19)/(20) reveals that a plot of i vs [S] should be linear, the slope of which provides a value of the lumped parameter Φ_k, where

$$\Phi_k \;=\; \left\{\frac{\phi}{k_0^{3/4}}\right\}\;\left\{1-\frac{1}{2a}\left(\frac{D_S}{k_0}\right)^{1/2}\right\} \tag{21}$$

Φ_k can also be determined from a single measurement as long as all pre-parenthesis terms in Eq. (20) are known. Knowledge of Φ_k as a function of the internal radius of the

ring allows construction of a Φ_k vs a^{-1} plot which should be a straight line with a (slope/intercept) value equal to $0.5(D_S/k_0)^{1/2}$, allowing determination of k_0. This can be used, in association with the slope or intercept of the Φ_k vs a^{-1} plot, to obtain ϕ. One further simplification can be achieved by noting that, when $\rho_0 > 5.5$

$$i = \frac{nFD_S^{3/4}\pi a^{1/2} I_{ph}\varepsilon_\lambda [S]\left(b^2 - a^2\right)^{1/2}}{1.03} \left\{\frac{\phi}{k_0^{3/4}}\right\} \qquad (22)$$

with an error of 10% with respect to Eq. (19). Use of Eq. (22) allows for the direct determination of $\phi/k_0^{3/4}$ from the slope of a plot of i vs [S], although care should be exercised in the use of this equation, given its error and range of utility ($20 > \rho_0 > 5.5$).

3.2 Theory for the Transport-Limited, Steady State Photocurrent from a PCE System

Having shown how the MORE can be used to completely characterize PE systems, let us now consider the behavior of PCE systems. The system to be modelled is shown in Eqs. (1a), (1c-1e). As in section 3.1, the steady state diffusion equation for S* and S^+ (the latter being the species that is detected at the electrode surface) are set up using the following assumptions 2.1-2.3. These are made in addition to assumptions 1.1-1.3.

2.1 the loss reaction, Eq. (1d), is pseudo- 1st order with respect to $[S^+]$ with rate coefficient k_2.

2.2 A is present in such large excess (a) that [A] is uniform in the vicinity of S/S* and that the electron transfer reaction (Eq. (1c)) is pseudo-first order with respect to [S*] i.e. either [S], ϕ or I_{ph} is small and so $k_1[A]$ can be considered constant; (b) the kinetics of electron transfer between S* and A are fast compared to those of mass transport of S*. Thus A reacts with S* before S* diffuses any significant distance.

2.3 The electron transfer kinetics of S^+ at the electrode are extremely rapid, so the photocurrent is under either mass transport or photochemical kinetic control.

The coupled diffusion equations for S* and S^+ inside the beam are then given by:

$$D_S \frac{\partial^2[S^*]}{\partial x^2} + D_S \frac{\partial^2[S^*]}{\partial r^2} + \frac{D_S}{r}\frac{\partial[S^*]}{\partial r} - (k_0 + k_1[A])[S^*] + \phi I_{ph}\varepsilon_\lambda[S]e^{-\varepsilon_\lambda[S]x} = 0 \quad (23a)$$

$$D_S \frac{\partial^2[S^+]}{\partial x^2} + D_S \frac{\partial^2[S^+]}{\partial r^2} + \frac{D_S}{r}\frac{\partial[S^+]}{\partial r} - k_2[S^+] + k_1[A][S^*] = 0 \quad (23b)$$

Using assumption 2.2, we can neglect terms in Eq. (23a) that refer to diffusion giving:

$$[S^*] = \frac{\phi I_{ph}\varepsilon_\lambda[S]e^{-\varepsilon_\lambda[S]x}}{(k_0 + k_1[A])} \quad (24)$$

Combining Eqs. (23b) and (24) gives that, inside and outside the beam respectively:

$$D_s \frac{\partial^2[S^+]}{\partial x^2} + D_s \frac{\partial^2[S^+]}{\partial r^2} + \frac{D_s}{r}\frac{\partial[S^+]}{\partial r} - k_2[S^+] + \phi' I_o\varepsilon_\lambda[S]e^{-\varepsilon_\lambda[S]x} = 0 \quad (25a)$$

$$D_s \frac{\partial^2[S^+]}{\partial x^2} + D_s \frac{\partial^2[S^+]}{\partial r^2} + \frac{D_s}{r}\frac{\partial[S^+]}{\partial r} - k_2[S^+] = 0 \quad (25b)$$

where $\phi' = \frac{k_1[A]}{k_0 + k_1[A]}\phi$. Eqs. (25) are analogous to Eqs. (2) and may be non-dimensionalised in the same fashion – except that expressions for χ, ρ and U (Eqs. (3-4)) are now written in terms of k_2, $X_{k,2}$, ϕ' and S^+. Non-dimensionalisation of Eqs. (25) yields expressions identical to Eqs. (5), U now corresponding to S^+ rather than S*. Conveniently, the non-dimensional diffusion equations for the PCE system are also subject to the same boundary conditions given in Table 1 and so may be solved by the same method as the one used for the PE system. Thus, when $20 > \rho_0 > 1$ & $\gamma < 1$:

$$i = \frac{2nFD_S\pi\phi I_{ph}\varepsilon_\lambda[S](b^2 - a^2)^{\frac{1}{2}}}{1.03k_2}\left(\frac{k_1[A]}{k_0 + k_1[A]}\right)\left(\frac{a}{X_{k,2}}\right)^{\frac{1}{2}}\left\{1 - \frac{a}{X_{k,2}}K_1\left(\frac{a}{X_{k,2}}\right)I_0\left(\frac{a}{X_{k,2}}\right)\right\} \quad (26)$$

or, when $20 > \rho_0 > 1$ & $\gamma < 1$, with an error of 4% with respect to eq (26):

$$i = \frac{nFD_S^{3/4}\pi a^{1/2}I_{ph}\varepsilon_\lambda[S](b^2 - a^2)^{1/2}}{1.03}\left(\frac{k_1[A]}{k_0 + k_1[A]}\right)\left\{\frac{\phi}{k_2^{3/4}}\right\}\left\{1 - \frac{1}{2a}\left(\frac{D_S}{k_2}\right)^{1/2}\right\} \quad (27)$$

or when $20 > \rho_0 > 5.5$ & $\gamma < 1$, with an error of 10% with respect to Eq. (26):

$$i = \frac{nFD_S^{3/4}\pi a^{1/2} I_{ph}\varepsilon_\lambda [S]\left(b^2 - a^2\right)^{1/2}}{1.03}\left(\frac{k_1[A]}{k_0 + k_1[A]}\right)\left\{\frac{\phi}{k_2^{3/4}}\right\} \quad (28)$$

When $k_1[A] >> k_0$ i.e. at larger scavenger concentration, $k_1[A]/(k_0+k_1[A]) \approx 1$ and Eqs. (26-28) reduce to Eqs. (19), (20) and (22) respectively (with k_2 replacing k_0). Alternatively, and using Eq. (27) as an example, we can write

$$\frac{1}{i} = \left(\frac{nFD_S^{3/4}\pi a^{1/2} I_{ph}\phi\varepsilon_\lambda [S]\left(b^2 - a^2\right)^{1/2}}{1.03k_2^{3/4}}\left\{1 - \frac{1}{2a}\left(\frac{D_S}{k_2}\right)^{1/2}\right\}\right)^{-1}\left(1 + \frac{k_0}{k_1[A]}\right) \quad (29)$$

from which it can be seen that a plot of i^{-1} vas $[A]^{-1}$ should be a straight line with a (slope/intercept) value equal to k_0/k_1. As in the case of the PE model, a plot of Φ_k vs a^{-1} should be a straight line from which, knowing k_0/k_1, values of k_2 and ϕ can be obtained. Finally, knowing k_0/k_1, and in accordance with Eq. (28), a simple plot of i vs [S] allows for the determination of $\phi/k_0^{3/4}$ when $\rho_0 > 5.5$.

3.3 Photoelectrochemical studies of the $Ru(bipy)_3^{2+}/Fe^{3+}$ system

Having modelled the photocurrent behaviour for both PE and PCE systems at the MORE let us, for illustration, briefly consider the application of those models to the $Ru(bipy)_3^{2+}$ / Fe^{3+} sensitiser / scavenger PCE system, which can be represented as [46]:

$$Ru(bipy)_3^{2+} \underset{k_o}{\overset{h\nu,\phi}{\rightleftharpoons}} Ru(bipy)_3^{2+*} \quad (30a)$$

$$Ru(bipy)_3^{2+*} + Fe^{3+} \xrightarrow{k'_1} Ru(bipy)_3^{3+} + Fe^{2+} \quad (30b)$$

$$Ru(bipy)_3^{3+} \xrightarrow{k_2} Ru(bipy)_3^{2+} \quad (30c)$$

The dependence of the measured photocurrent, which is due to the reduction of $Ru(bipy)_3^{3+}$, on (scavenger) $[Fe^{3+}]$ is shown in Fig. 6. As discussed in relation to Eq.

(29), the reciprocal photocurrent should be proportional to $[Fe^{3+}]^{-1}$ with a slope/intercept value numerically equal to k_0/k_1. This in turn corresponds to $1/K_{SV}$, the reciprocal Stern-Volmer coefficient for the $Fe^{3+}/Ru(bipy)_3^{2+}$ system [47]. Using the data of Fig. 6, Fig. 7 shows that this theoretically predicted dependence is also observed experimentally (R^2 = 0.992), giving $k_1/k_0 = K_{sv} = 0.36$ m^3 mol^{-1}. This is in good agreement with a literature value of $K_{SV} = 0.9$ m^3 mol^{-1} [47] and, in conjunction with the linearity of the plot in Fig. 7, confirms the applicability of our model and the expressions of Eqs. (26)/(29).

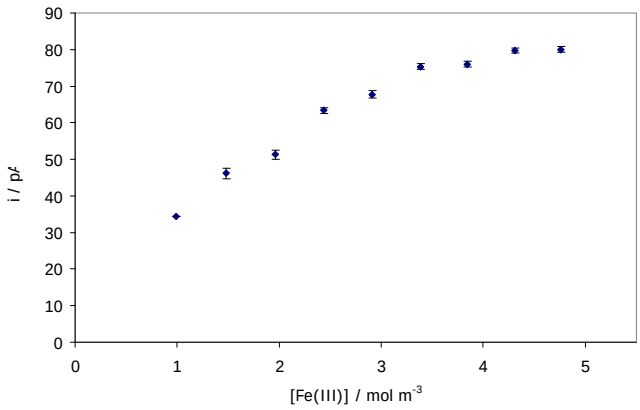

Fig. 6. Photocurrent observed from $Ru(bipy)_3^{2+}/Fe^{3+}$ system at a MORE as a function of $[Fe^{3+}]$. $[Ru(bipy)_3^{2+}]$ = 10 mol m^{-3}; λ = 460nm; electrode potential = +0.5 V vs. SCE. Minimum signal-to-noise ratio = 27.

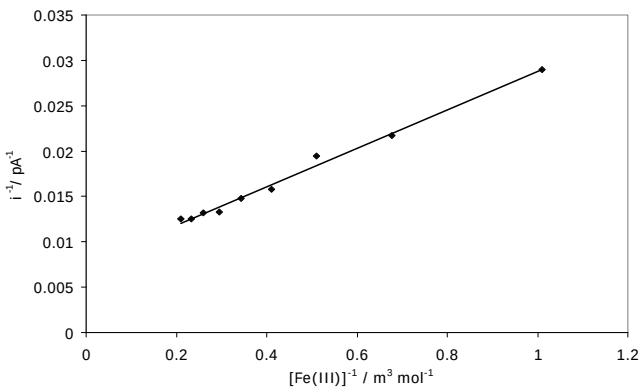

Fig. 7. Data of Fig. 6 plotted in accordance with Eq. (29)

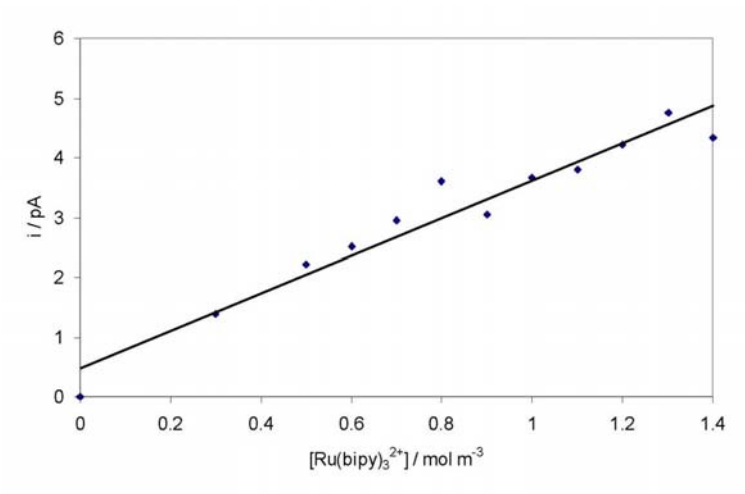

Fig. 8. Photocurrent observed at MORE from $Ru(bipy)_3^{2+}/Fe^{3+}$ system as a function of $[Ru(bipy)_3^{2+}]$. $[Fe^{3+}] = 5$ mol m^{-3}; $\lambda = 460$nm; electrode potential = +0.5 V vs. SCE**.** Minimum signal-to-noise ratio = 2. All data with S/N < 2 discarded.

Eqs. (26-28) predict that the photocurrent should be linearly proportional to $[Ru(bipy)_3^{2+}]$. Fig. 8 confirms that this is the case, again supporting the validity of Eqs (26-28). Knowing k_0/k_1 and all other experimental parameters, it is possible, by use of Eq. (28), to extract from the slope of Fig. 8 a value of $\phi/k_2^{3/4}$ which, for those data, is found to be equal to 5.81 $s^{3/4}$. Provided k_2 is known, it is then possible to calculate a value for the quantum efficiency for the photoexcitation and intersystem crossing of $Ru(bipy)_3^{2+*}$. However, in order to perform this calculation, we must first determine a value for k_2. As mentioned in sections 3.2, k_2 may be obtained by measuring the photocurrent as a function of a, the inner radius of the ring. This requires the time consuming fabrication of a range of MOREs with inner radii values spread over at least two orders of magnitude. However, comparison between this mathematical model for PE/PCE systems at the MORE and our earlier model for the same systems at an ODE [31,32] leads us to believe that both k_0 and k_2 can be more readily obtained for PE and PCE systems by simply studying the time-dependence of the light-on photocurrent transients. This will be explored in the next paper in this series.

4. Conclusions

We have derived asymptotic analytical expressions for the steady state, transport limited photocurrent generated by PE and PCE systems at MOREs with thin microrings ($a/b > 0.99$). The expressions were generated by solving the diffusion equation for the photogenerated electroactive species both inside and outside the beam, and matching the solutions at the beam surface. The expressions are used to design experimental protocols that allow for the complete characterization of a system's kinetics. The MORE, the expressions and the associated protocols will therefore be highly useful in the study of a range of homogeneous and microheterogeneous photoelectrochemical systems.

The expressions were tested by using them to interpret the results of a MORE study of the $Ru(bipy)_3^{2+}/Fe^{3+}$ system. The value of the Stern-Volmer constant for the quenching of photoexcited $Ru(bipy)_3^{2+}$ by Fe^{3+} so obtained (0.36 m^3 mol^{-1}) compares favourably with the value obtained from fluorescence measurements (0.9 m^3 mol^{-1}). We are currently studying the transient response of PE and PCE systems at the MORE.

Acknowledgements

We thank the University of Central Lancashire (UCLan) for a postgraduate research studentship for F.A. and a period of Sabbatical leave for C.B. We also thank the EM Facility at the University of Brighton for help with the manufacture of the MOREs and Drs Dave Parker (UCLan) and Ben Horrocks (University of Newcastle-Upon-Tyne) for helpful discussions.

Appendix

Fig. 2 illustrates the geometry of the problem solved in section 3.1. It is assumed that the optical disc is uniformly illuminated by parallel light passing from the disc into solution. An explanation of this assumption and its limitations is given here.

The MORE is most conveniently made by coating a fibre optic with a layer of an appropriate conductor [1,18,19], such as gold. The fibre itself consists of a central dielectric core of refractive index n_1, surrounded by a concentric cladding of a slightly lower (by ≅1%) refractive index, n_2. The numerical aperture, NA, of the fibre is given by

$$NA = \sin\alpha = \left(n_1^2 - n_2^2\right)^{1/2} \qquad \text{(A1)}$$

where α, which is measured with respect to the central axis of the fibre, is the semi-apex angle of the cone shape formed by the divergence of light as it leaves the fibre. Light entering the fibre at an angle less than α is propagated down the core of the fibre through total internal reflectance at the core-cladding interface. The model of the light beam emerging from the optical disc presented in Fig. 2 therefore appears to be at variance with the physical reality in two ways:

1. The light emerges not as a parallel beam, but rather as a divergent cone; and
2. Light is propagated down the core, not the cladding, giving rise at the surface of the optical disc to a “dark zone” between the core and the innermost edge of the ring.

The latter concern can be dismissed by consideration of the actual construction of the MORE, Fig. 1. The length of fibre optic employed is usually no more than 7 cm and is held straight along its entire length. Light may therefore be transmitted through the cladding, an expectation confirmed by our earlier study of the electrochemistry of the phenothiazinium dye, methylene blue (MB^+), wherein the photoexcited triplet state of the dye was detected by direct electrochemical oxidation at the ring of the MORE [1]. The thickness of the cladding of the fibres used in all MORE experiments was 25 μm. $^3MB^+$ has a lifetime of 90 μs[48] and a diffusion coefficient of 8.1 x 10^{-10} m^2 s^{-1} [49] – thus, the maximum radial distance that $^3MB^+$ might be expected to diffuse after leaving the beam and before relaxation to its ground state is 270 nm. This is ~1% of the thickness of supposed “dark zone” between the core and the ring, indicating that a

significant intensity of light is transmitted through the cladding. This light will be attenuated if the fibre is either bent or is significantly longer than the length used in Fig. 1 and experimentalists should bear this in mind when using their own MOREs.

The effect of the former concern can be understood by consideration of the systems kinetic length, generically X_k, specifically $X_{k,0}$ or $X_{k,2}$ (consideration in terms of the absorbance length, X_ε, is inappropriate as we assume light is virtually unattenuated as it passes through solution i.e. $\gamma << 1$). To a first approximation, only that material generated within X_k of the surface of the MORE can be detected on the ring. The spread of the beam at X_k, given by the ratio of the radius of the beam r_B to a is:

$$\frac{r_B}{a} = 1 + \frac{X_k}{a}\tan\left(\arcsin(NA)\right) \qquad \text{(A2)}$$

Commercially available fibres have NA ≅ 0.1-0.4. In that range, and in non-dimensionalised form,

$$\frac{\rho_B}{\rho_0} = 1 + \frac{NA}{\rho_0} \qquad \text{(A3)}$$

Eqs. (19) & (26) are valid over the range $20 > \rho_0 > 1$. In conjunction with the above limits on NA, this gives minimum and maximum divergences of 1.005 or 0.5% and 1.4 or 40% respectively. It should be realized that some spread is actually desirable as it provides extra validation for the assumption made in solving Eq. (11) i.e. that Eq. (11) is assumed to hold in the space over the ring. However, in order that the assumption of an invariant light intensity at $x < X_k$ should hold (i.e. $\gamma < 1$), it would seem appropriate to restrict use of fibre optic based MOREs to those systems where the divergence is no more than 1.1 or 10% i.e. that NA/ρ_0 is no more than 0.1. Again, experimentalists should bear this restriction in mind when using their own MOREs.

Figure Captions

Fig. 1. Schematic cross section of tip of MORE and home-made light coupling unit.

Fig. 2. The cylindrical polar geometry of the MORE problem

Fig. 3. Concentration profile of photogenerated species (as U/γ^2) at MORE surface inside and outside the beam, calculated using Eqs. (10) when $\gamma < 1$ and the ring is off. Calculated for ρ_0=2.5 and γ=0.1. Solid line represents U/γ^2 as given by Eq. (10a), broken line as given by Eq. (10b).

Fig. 4. Percentage error associated with using Eq. (10a) rather than Eq. (10b) to calculate concentration of photogenerated species (as U) in the space defined by $\rho_0 < \rho < 1.01\rho_0$ over an illuminated MORE with the electrochemical ring switched off.

Fig. 5. Concentration profile of photogenerated species (as U / γ^2) at the MORE surface, as a function of ρ and χ, calculated using Eq. (17) when ρ_0=2.5 and γ=0.5 and the electrochemical ring is switched on.

Fig. 6. Photocurrent observed from $Ru(bipy)_3^{2+}$ / Fe^{3+} system at a MORE as a function of $[Fe^{3+}]$. $[Ru(bipy)_3^{2+}]$ = 10 mol m^{-3}; λ = 460nm; electrode potential = +0.5 V vs. SCE. Minimum signal-to-noise ratio = 27

Fig. 7. Data of Fig. 6 plotted in accordance with Eq. (29).

Fig. 8. Photocurrent observed at MORE from $Ru(bipy)_3^{2+}/Fe^{3+}$ system as a function of $[Ru(bipy)_3^{2+}]$. $[Fe^{3+}]$ = 5 mol m^{-3}; λ = 460nm; electrode potential = +0.5 V vs. SCE. Minimum signal-to-noise ratio = 2. All data with S/N < 2 discarded.

References

[1] G.I.Pennarun, C.Boxall, D.O'Hare, Analyst 121 (1996) 1779.

[2] C.G.Zoski, Electroanalysis 14 (2002) 1041.

[3] J.Janata, M.Josowicz, P.Vanýsek, D.M.DeVaney, Anal. Chem. 70 (1998) 179R.

[4] J.V.Macpherson, P.R.Unwin, Anal. Chem. 70 (1998) 2914.

[5] J.V.Macpherson, N.Simjee, P.R.Unwin, Electrochim. Acta, 47 (2001) 29.

[6] S.Fonseca, S.Ahmed, T.J.Kemp, P.R.Unwin, Photochem. Photobiol. Sci. 2 (2003) 98.

[7] Y.Lee, S.Amemiya, A.J.Bard, Anal. Chem. 73 (2001) 2261.

[8] Y.Lee, A.J.Bard, Anal. Chem. 74 (2002) 3626.

[9] Y.Lee, Z.Ding, A.J.Bard, Anal. Chem. 74 (2002) 3634.

[10] S.Szuneritis, D.R.Walt, Anal. Chem. 74 (2002) 1718.

[11] P.J.S.Smith, P.G.Haydon, A.Hengstenberg, S.K.Jung, Electrochim. Acta 47 (2001) 283.

[12] N.Casillas, P.James, W.H.Smryl, J. Electrochem. Soc. 132 (1995) L16.

[13] G.Shi, L.F.Garfias-Mesias, W.H.Smyrl, J. Electrochem. Soc. 145 (1998) 2011.

[14] B.A.Brookes, D.J.Gavaghan, R.G.Compton, J. Phys. Chem. B 106 (2002) 4886.

[15] L.S.Kuhn, A.Weber, S.G.Weber, Anal. Chem. 62 (1990) 1631.

[16] Q.Zhung, H.Che, Electroanalysis 6 (1994) 485.

[17] C.B.Cohen, S.G.Weber, Anal. Chem. 65 (1993) 169.

[18] G.I.Pennarun, C.Boxall, D.O'Hare in: A.J.Ricco, M.A.Butler, P.Vanysek, G.Horvai and A.F.Silva (Eds.), Proceedings of the Symposium on Chemical and Biological Sensors and Analytical Electrochemical Methods, 192nd Meeting of the Electrochemical Society, The Electrochemical Society, Pennington NJ, 1997, p.1039.

[19] F.Andrieux, C.Boxall, S.Xiao, D.O'Hare in: M.A.Butler, P.Vanysek and N.Yamazoe (Eds.), Proceedings of the Symposium on Chemical and Biological Sensors and Analytical Methods II, 200th Meeting of the Electrochemical Society, The Electrochemical Society, Pennington NJ, 2001, pp.531.

[20] A.Szabo, J. Phys. Chem. 91 (1987) 3108.

[21] J.S.Symanski, S.Bruckenstein, J. Electrochem. Soc. 135 (1998) 1985.

[22] M.Fleishmann, S.Pons, J. Electroanal. Chem. 222 (1987) 107.

[23] M.Fleishmann, S.Bandyopadhyay, S.Pons, J. Phys. Chem. 89 (1985) 5537.

[24] C.G.Philips, H.A.Stone, J. Electroanal. Chem. 396 (1995) 277.

[25] D.K.Cope, D.E.Tallman, J. Electroanal. Chem. 303 (1991) 1.

[26] D.K.Cope, C.H.Scott, D.E.Tallman, J. Electroanal. Chem. 289 (1989) 49.

[27] U.Kalpathy, D.E.Tallman, J. Electroanal. Chem. 325 (1992) 65.

[28] D.E.Tallman, Anal. Chem. 66 (1994) 557.

[29] Z.Wu, Z.Zhang, Acta Chim. Sin. 51 (1993) 239.

[30] Z.Wu, Z.Zhang, Acta Chim. Sin. 51 (1993) 697.

[31] C.Boxall, W.J.Albery, Phys. Chem. Chem. Phys. 2 (2000) 3631.

[32] C.Boxall, W.J.Albery, Phys. Chem. Chem. Phys. 2 (2000) 3651.

[33] M.R.Hoffman, S.T.Martin, W.Choi, D.Bahnemann, Chem.Rev. 95 (1995) 69.

[34] A.L.Linsebigler, G.Lu, J.T.Yates Jr., Chem.Rev. 95 (1995) 735.

[35] P.Kamat, Chem.Rev. 93 (1993) 267.

[36] A.Hagfeldt, M.Grätzel, Chem.Rev. 95 (1995) 49.

[37] T.L.Rose et al. in: Proceedings of the Symposium on Water Purification by Photocatalytic, Photoelectrochemical and Electrochemical Processes, The Electrochemical Society, Pennington, NJ, 1994.

[38] Y.Wang, Acc.Chem.Res. 24 (1991) 133.

[39] D.R.Deaver, Nature, 377(6551) (1995) 758.

[40] E.M.Tuite, J.M.Kelly, J.Photochem.Photobiol.B:Biol. 21 (1993) 103.

[41] M.Abramowitz, I.A.Stegun, Handbook of Mathematical Functions, Dover Publications, NY, 1965, p 374.

[42] G.N.Watson, A Treatise on the Theory of Bessel Functions, 2nd ed., Cambridge University Press, Cambridge UK, 1944.

[43] M.Abramowitz, I.A.Stegun, Handbook of Mathematical Functions, Dover Publications, NY, 1965, p.375, eq 9.6.15.

[44] M.Abramowitz, I.A.Stegun, Handbook of Mathematical Functions, Dover Publications, NY, 1965, p.487, eq 11.4.37.

[45] A.Jeffrey, Handbook of Mathematical Formulas and Integrals, Academic Press, London, 1995, p.274, eqs 17.9.1.1.1-17.9.1.1.2.

[46] W.J.Albery, A.Foulds, J. Photochem. 10 (1979) 41.

[47] C.T.Lin, N.Sutin, J. Phys. Chem. 80 (1976) 97.

[48] J.Faure, R.Bonneau, J.Jousott-Dubien, J.Photochem.Photobiol. 6 (1967) 331.

[49] P.R.Unwin, A.J.Bard, Anal.Chem. 64 (1992) 113